Rare Metal Materials and Engineering
Volume 49, Issue 3, March 2020
Available online at www.rmme.ac.cn

Science Press

Cite this article as: Rare Metal Materials and Engineering, 2020, 49(3): 0833-0841.

ARTICLE

Calculation of Flow, Heat Transfer and Evaporation during the Electron Beam Cold Hearth Melting of Ti-6Al-4V Alloy

Cen Mengjiang, Liu Yuan, Chen Xiang, Zhang Huawei, Li Yanxiang

Key Laboratory for Advanced Materials Processing Technology (MOE), Tsinghua University, Beijing 100084, China

Abstract: Electron beam cold hearth melting (EBCHM) is a promising technique for achieving premium titanium alloys for critical rotating parts of the aero-engine and to recycle the titanium scraps. This paper studied the heat transfer, the fluid flow and solidification in the cold hearth during EBCHM process of Ti-6Al-4V alloy. The results show that the melt is constrained to a very shallow depth which is 15 mm in our experiment and the melt velocity is about a few centimeters per second. The melt temperature increases with the increase of melting power and decreases with the increase of melting rate. The melt depth increases with the increase of melting power, while the effect of melting rate on the shape of melt pool is not obvious. The trajectories of inclusions with different densities and sizes were simulated. The density has great influence on the trajectories of particles. The evaporation model was established to study the influence of melting parameters on the ingot composition. The results indicate that melting temperature, melting rate and composition of row materials have great influence on the ingot composition. Round ingots were produced by the commercial EBCHM furnace in the factory. The morphology of the shell was investigated and the ingot composition was tested. The calculating results are in good agreement with experiment.

Key words: EBCHM; Ti-6Al-4V; simulation; evaporation

Titanium alloys have a series of excellent properties, such as low density, prominent corrosion and fatigue resistance, high-temperature strength, excellent fracture toughness, and low Young's modulus[1-3]. The demands for titanium alloys in aerospace and marine applications are increasing rapidly. The melting methods of titanium alloys mainly include vacuum self-consuming arc melting (VAR), electron beam cold hearth melting (EBCHM), plasma beam cold hearth melting (PAM) and vacuum induction melting (VIM)[4-6]. As the most important melting method, VAR can remove dissolved gases and minimize macro-segregation, which is conductive to improving ingot quality. Nevertheless, the main drawback of VAR is that it cannot effectively remove the inclusions in melt and such inclusions directly result in failure and fracture of most parts. Compared to VAR, EBCHM has the following advantages[7-10]: (1) The melt flow conditions in the cold hearth lead to a long residence time of inclusions in molten metal, which promotes dissolution of inclusions; (2) The source of raw materials is relatively wide, which can be titanium sponges, cutting wastes and recycled titanium scraps; (3) The melting chamber has high vacuum (typically 10^{-2}~10^{-3} Pa), which results in evaporation of volatile impurities; (4) The possibility to produce large-scale ingots is not only of round but also of rectangular cross section.

Thus, EBCHM was gradually applied to melt titanium alloys after the 1980s. As so many merits mentioned above, EBCHM or combining EBCHM and VAR has become a tendency to produce high quality titanium ingots.

The growing industrial interests in the electron beam melting and refining processes have been illustrated by abundant literatures. The temperature distribution and melt flow in the crystallizer were investigated[11]. The cold hearth is also a very important component of EBCHM fur-

Received date: March 29, 2019
Foundation item: National Key R&D Program of China (2016YFB0301200)
Corresponding author: Liu Yuan, Ph. D., Associate Professor, School of Materials Science and Engineering, Tsinghua University, Beijing 100084, P. R. China, Tel: 0086-10-62789328, E-mail: yuanliu@mail.tsinghua.edu.cn

nace for purifying molten metal and controlling evaporation. Isawa et al[12] observed the melt flow in the hearth and found the flow was relatively strong. Bellot el al[13] developed a comprehensive model of the cold hearth based on coupled momentum, solute, and heat transport equations. The model calculated the velocity, turbulence intensity, temperature, and alloy composition in the liquid and the solid phase. The behavior of a hard-alpha inclusion during melting was also concerned. The velocity field was studied by melting alloy button using electron beam furnace[14,15]. The results show that Marangoni flow caused by surface tension gradient is the dominant flow. Bellot et al[16] established a numerical model of the dissolution process of Ti-N inclusions based on the diffusion of nitrogen and the migrating of interface. Han et al[17] studied the effect of EBCHM furnace on the removal of TiN inclusions and found the cold hearth can effectively remove this kind of inclusions. Ghassan et al[18] investigated the dissolution of high density inclusions in titanium alloys. Akhonin et al[19] investigated the effect of melting power and melting rate on the temperature of cold hearth and crystallizer. The results indicate that the melt temperature in the hearth decreases and that in the crystallizer increases with an increase of the melting rate for a given electron beam power. An increase in the electron beam melting power leads to an increase in the melt temperature and the effect is much greater in the hearth compared to the crystallizer.

However, the previous experimental studies are mainly concerned with alloy buttons or small ingots. The EBCHM furnaces used previously are small in size and power, which does not accord with the production reality. Also, the flow field in the cold hearth is not analyzed. In this paper, the flow field, temperature field and solidification in the cold hearth during melting Ti-6Al-4V alloy were simulated by the commercial software Ansys Fluent. Round ingots were produced by the commercial EBCHM furnace. The morphology of the shell was measured and the ingot composition was tested to verify the calculating results.

1 Establishment of the Mathematical Model

1.1 Assumptions

The EBCHM furnace used in this paper is shown in Fig.1. Due to very high energy of electron beam, temperature gradient is generated on the melt surface. As surface tension of melt has approximately a linear relationship with temperature, surface tension gradient exists on the surface. Under the effect of surface tension and inhomogeneity of density, the melt presents a complex flow.

Due to the complex nature of EBCHM mentioned above, following assumptions are made in this study to simplify the model: (1) The heat flux on the surface of melt is considered homogeneous, as the scan frequency is big enough in order to reduce evaporation; (2) The distortion of melt on the surface is not considered and the surface is treated as flat; (3) Material physical properties such as thermo-conductivity, specific heat, viscosity do not change with temperature.

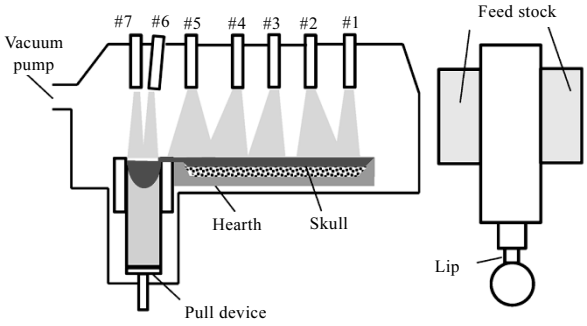

Fig.1 Schematic diagram of EBCHM furnace

1.2 Physical model of simulation

Calculating is carried out on a three-dimensional meshed geometry model. As the melting reaches stable, the model is a representation of the molten metal and solidified shell. Due to the molten pool is very shallow and the size of cold hearth is very large, the dense grids are adopted in the molten metal, while sparse grids are used in the shell part to improve the calculation accuracy and save computation time. The inlet is divided into fine meshes to reduce calculating error, as shown in Fig.2.

It is known from the melting process that the physical phenomena have to be considered in the simulation, including the heat flux of electron beam, thermal radiation of the melt surface, phase change, heat exchange of cold hearth, the buoyancy of the melt produced by temperature gradient, surface tension caused by surface temperature gradient, turbulence, the interaction between melt and solid phase in the paste region. Therefore, the physical models that needs to be used include continuity equation, energy equation, solidification model and surface tension model.

The mass conservation equation (continuity equation) can be expressed as:

$$\frac{\partial \rho}{\partial t} + \nabla \cdot \left(\rho \vec{v} \right) = S_{\mathrm{m}} \tag{1}$$

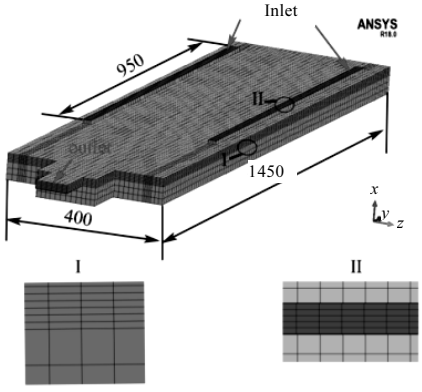

Fig.2 3D physical model used for simulation

where S_m is the mass source, representing the mass flow rate from the second phase into the melt or from the melt into other phases; ρ is the density of melt; t is the time; $\vec{v}$ is the velocity of melt.

In this study, external forces applied on the defined domain include gravity and surface tension. Momentum conservation equation (in inertial reference frame) is shown as:

$$\frac{\partial}{\partial t}\left(\rho\vec{v}\right)+\nabla\cdot\left(\rho\vec{v}\vec{v}\right)=-\nabla p+\nabla\cdot\left(\tau\right)+\rho\vec{g}+\vec{F} \quad (2)$$

where p is static pressure; τ is the stress tensor; $\vec{g}$ is the acceleration of gravity; $\vec{F}$ is the extra volume force.

In the present work, the electron beam energy is inserted into the domain from the top surface and is used to increase the domain temperature. At the same time, heat loss by conduction, convection and radiation occurs through the boundaries. The conservation of energy is presented as:

$$\frac{\partial}{\partial t}(\rho E)+\nabla\cdot\left(\vec{v}(\rho E+p)\right)=\nabla\cdot\left(k_{\text{eff}}\nabla T-\sum_j h_j\vec{J}_j+\left(\tau_{\text{eff}}\cdot\vec{v}\right)\right)+S_h \quad (3)$$

where k_{eff} is effective thermal conductivity; $\vec{j}_j$ is the diffusion flux of matter j; The three on the right represent energy transfer through heat conduction, material diffusion and viscous decay; S_h is the volume heat source; E and h_j are function of material properties.

For solidification and melting process, the enthalpy of material can be expressed as the sum of sensible enthalpy and latent heat:

$$H=h+\Delta H \quad (4)$$

where ΔH is the temperature dependent function of the latent heat that is gradually added into the domain by increasing the temperature from solidus to liquidus temperature; h is the temperature dependent term of enthalpy and is defined as:

$$h=h_{\text{ref}}+\int_{T_{\text{ref}}}^{T}c_p\mathrm{d}T \quad (5)$$

where h_{ref} is the reference enthalpy; T_{ref} is the reference temperature; c_p is the specific heat under certain pressure.

The paste area is treated by enthalpy-porous method, which treat the paste area as porous medium and the pore volume of each unit is equal to the liquid fraction of the unit. In the fully solidified area, the pore volume is zero, which also makes the velocity of the region zero, and the momentum generated by the decrease of pore volume in the paste region is as follows:

$$S=\frac{(1-\beta)^2}{(\beta^3+\varepsilon)}A_{\text{mush}}\left(\vec{v}-\vec{v}_p\right) \quad (6)$$

where β is the liquid volume fraction; ε is a small number; A_{must} is mushy zone constant; $\vec{v}_p$ is the drawing rate of solidified part for continuous casting. The liquid fraction β is defined as:

$$\beta=\begin{cases}0 & T<T_s\\ \dfrac{T-T_s}{T_l-T_s} & T_s<T<T_l\\ 1 & T>T_l\end{cases} \quad (7)$$

where T is the melt temperature; T_s is the solidus line; T_l is the liquidus line. So enthalpy change ΔH of solidification can be expressed as:

$$\Delta H=\beta L \quad (8)$$

where L is latent heat of the material.

The trajectories of discrete phase particles are predicted by integrating the force balance on the particle. This force balance can be written as:

$$\frac{\mathrm{d}\vec{u}_p}{\mathrm{d}t}=F_D\left(\vec{u}-\vec{u}_p\right)+\frac{\vec{g}\left(\rho_p-\rho\right)}{\rho_p}+\vec{F} \quad (9)$$

where $\vec{F}$ is an additional acceleration (force/unit particle mass) term; $F_D\left(\vec{u}-\vec{u}_p\right)$ is the drag force per unit particle mass.

The thermal conductivity and viscosity of Ti-6Al-4V were calculated by the data base of software ProCast as 36 $\text{W}\cdot(\text{m}\cdot\text{K})^{-1}$ and 0.0013 $\text{kg}\cdot(\text{m}\cdot\text{s})^{-1}$, respectively.

The specific heat C_p ($\text{J}\cdot(\text{K}^{-1}\cdot\text{mol})^{-1}$) is a function of temperature and usually can be fitted according to experimental data[20]:

$$C_p=a+b10^{-3}T+c10^5T^2+d10^{-6}T^2 \quad (10)$$

where a, b, c and d are characteristic constants of materials.

The surface tension of melt changes with temperature and composition. In the present work, the influence of composition is neglected. Schneider et al[21] measured the surface tension of Ti-6Al-4V melt by oscillating drop technique. A surface tension-temperature linear function can be obtained by the least square method:

$$\gamma=1.389\pm0.09-0.907\times10^{-4}\pm5.64\times10^{-5}\left(T-1660\ ^{\circ}\text{C}\right)(\text{N}\cdot\text{m}^{-1}) \quad (11)$$

where γ is the surface tension of melt; T is the melt temperature. The surface tension of melt has approximately a linear relationship with temperature and the coefficient is taken as –0.0009 $\text{N}\cdot(\text{m}\cdot\text{K})^{-1}$ according to Eq.(11).

The transfer of heat in the copper-shell interface is realized by conduction and radiation of gas gap. The heat transfer coefficient was selected as 600 $\text{W}\cdot(\text{m}^{-2}\cdot\text{K})^{-1}$ according the work of Kobryn[22].

1.3 Mathematical model of evaporation

The commercial EBCHM furnace usually have very long hearth, but many studies treat the melt of the hearth as homogeneous when calculating the evaporation. This treatment is obvious inaccurate. In the present work, the hearth was divided into different areas. The composition in one area is treated as homogeneous, while composition of different areas is different. The schematic graph of this method is shown in Fig.3.

The principle of mass conservation is used in the i^{th} area, then Eq.(12) is easy to get.

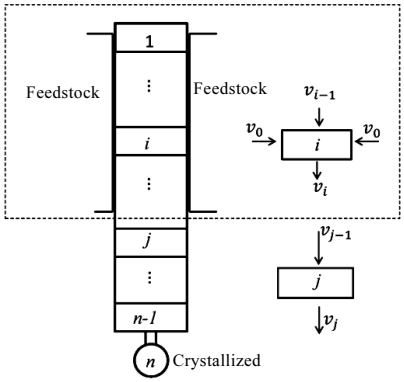

Fig.3 Schematic graph of dividing of the cold hearth

$$\begin{cases} v_i[X]_i = v_{i-1}[X]_{i-1} + 2v_0[X]_0 - A_i J_X^i \\ v_i[Y]_i = v_{i-1}[Y]_{i-1} + 2v_0[Y]_0 - A_i J_Y^i \\ v_i[Z]_i = v_{i-1}[Z]_{i-1} + 2v_0[Z]_0 - A_i J_Z^i \\ [X]_i + [Y]_i + [Z]_i = 1 \end{cases} \quad (12)$$

where v_i is the quantity of fluid flowing out of the i^{th} area in unit time; $[X]i$, $[Y]i$, $[Z]i$ are the mass fraction of the three elements (X, Y, Z represent three elements); v_{i-1} is the quantity of fluid flowing into the i^{th} area from the last area in unit time; v_0 is the quantity of fluid flowing into the i^{th} area from the feeding port in unit time; $[X]_0$, $[Y]_0$, $[Z]_0$ are the mass fraction of the three elements in the raw material; A_i is the area of the i^{th} area; J_X^i, J_Y^i, J_Z^i are the evaporation rate of the three elements.

As can be seen from Eq.(12), it is required to get the evaporation rate of the elements to calculate the melt composition. According to evaporation process, the evaporation of elements from melt into chamber depends upon the following three stages: (1) Atoms in the melt travel across the molten metal and reach the melt surface through convection diffusion; (2) Physical-chemical reaction takes place on the melt surface; (3) Atoms travel across the gas boundary layer and reach the distant chamber.

Fig.4 is a schematic describing of the elements travelling from the molten metal into the vacuum chamber. The meaning of each symbol is detailed in the mass transfer theory described below. As the atmosphere pressure in the vacuum chamber is very low, generally in the range of 0.01~0.1 Pa, mass transfer in the gas phase was neglected in this research.

According to the definition of mass transfer coefficient, evaporation rate of the gas-melt interface J_s can be expressed by Eq.(13).

$$J_s = k_s C_i^s \quad (13)$$

where C_i^s is the concentration of elements on the surface of melt and can be expressed as:

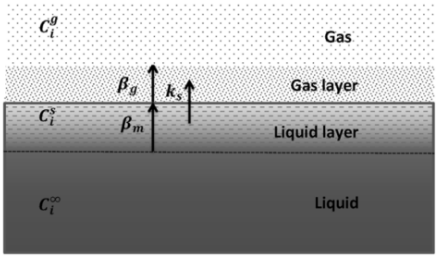

Fig.4 Schematic graph of evaporation process

$$C_i^s = \frac{X_i^s M_i}{V_m^s} \quad (14)$$

Evaporation rate J_s can be calculated according to Langmuir equation[21]:

$$J_s = \alpha_C p_i^0 \gamma_i X_i^s \sqrt{M_i / 2\pi RT} \quad (15)$$

According to Eq.(13)~Eq.(15), the interface mass transfer coefficient can be expressed by Eq.(16).

$$k_s = \frac{J_s}{C_i^s} = \frac{\alpha_C p_i^0 \gamma_i V_m^s}{\sqrt{2\pi RTM_i}} \quad (16)$$

Eq.(13) to Eq.(16) describe the evaporation of the melt-gas interface. The meanings of coefficients of these equations are summarized as shown in Table 1.

According to mass transfer theory of melt, the transfer rate (J_m) of elements in the melt can be expressed as:

$$J_m = \beta_m \left(C_i^\infty - C_i^s\right) \quad (17)$$

where β_m is the mass transfer rate of melt; C_i^∞ and C_i^s are concentration of element in the internal melt and on the melt surface, respectively.

Table 1 Coefficients and their meanings of Eq.(13)~Eq.(16)

Coefficients	Meaning
J_s	Evaporation rate on the gas-melt interface
k_s	Interface mass transfer coefficient
C_i^s	The concentration of i^{th} element on the melt surface
α_C	Condensation coefficient
p_i^0	The saturated vapor pressure of i^{th} element
γ_i	The activity coefficient of i^{th} element
X_i^s	Molar fraction of i^{th} element
M_i	The molar mass of i^{th} element
R	Gas constant
T	Melt temperature
V_m^s	Molar volume of surface melt

As substances can not accumulate in the process of transfer when melting reaches stable, Eq.(18) is easy to get:

$$J_m = J_s = J \quad (18)$$

where J is the total mass transfer coefficient of the evaporation process and can be expressed as:

$$J = \left(\frac{1}{\beta_m} + \frac{1}{k_s} \right)^{-1} C_i^{\infty} \quad (19)$$

The most important parameter in this evaporation model is activity coefficient (γ_i). In our previous work, the model of the activity coefficient of multi-component alloys were established by thermodynamics theory of alloys.[23]

2 Results and Discussion

The actual EBCHM furnace used to melting is shown in Fig.5. The main parameters are shown in Table 2. Two intersections, depicted as AA' and BB', are selected to show the result.

2.1 Melt pool characteristics

In the initial stage of melting, the melt contacts the hearth directly. With the melting progressing, the melt contacting the hearth solidifies and a shell forms. When the melting reaches stable, the fraction of solid and liquid will not change. The morphology of shell affects the flow of melt, the removal of inclusions and transfer of evaporating elements in the melt. The shell morphology was simulated, as shown in Fig.6 and Fig.7. It can be seen that the melt is constrained to a very shallow depth which is about 15 mm. The simulated and experimental results accord well.

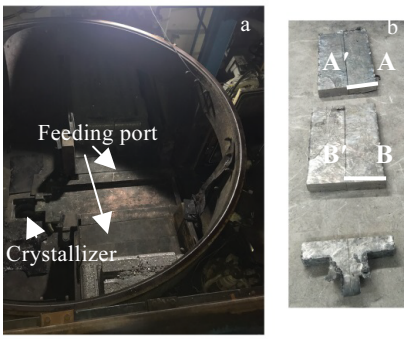

Fig.5 EBCHM furnace (a) and shell (b)

Table 2 Major parameters of melting

Parameters	Value
Hearth dimensions/mm	1450(L)×400(W)
Crystallizer diameter/mm	Φ260
Electron gun power/kW	450×7
Row material/wt%	Ti-9Al-4V
Ingot dimension/mm	Φ260×8100
Total melting power/kW	684
Pull rate/mm·min^{-1}	17.3

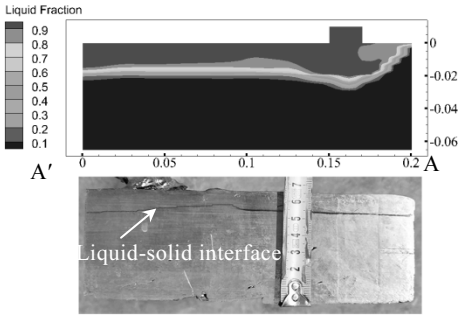

Fig.6 Simulated and experimental morphology of the shell (intersection A-A′)

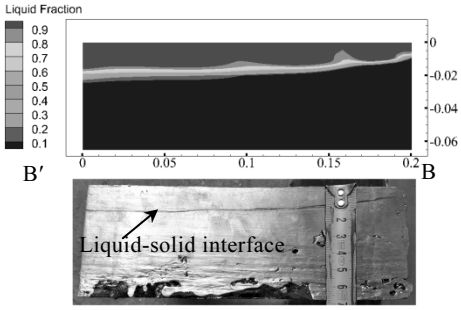

Fig.7 Simulated and experimental morphology of the shell (intersection B-B′)

The effect of melting power and melting rate on the morphology of molten pool was calculated, as shown in Fig.8 and Fig.9. It can be seen that the melt depth increases with the increase of melting power. However, the effect of melting rate on the morphology of molten pool is not obvious.

Melting temperature is a very important parameter during the EBCHM. One of the most important problems concerned during the EBCHM is the evaporation of elements with high saturated vapor pressure. Temperature is an import parameter affecting evaporation. In the present work, the scan pattern and scan frequency of electron beam are not

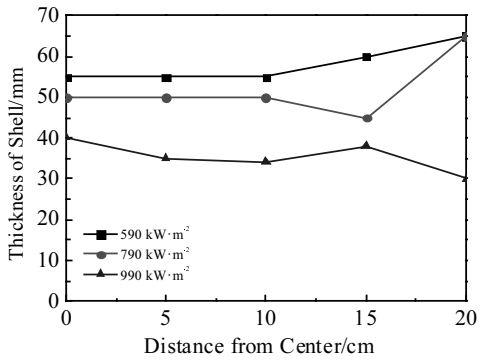

Fig.8 Effect of melting power on the melt depth

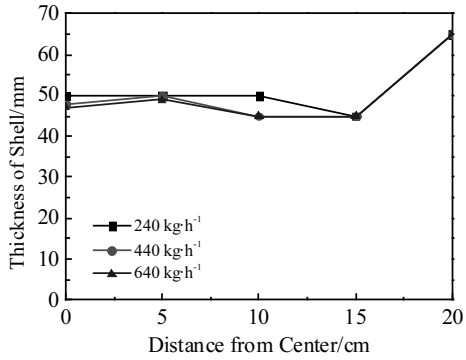

Fig.9 Effect of melting rate on the melt depth

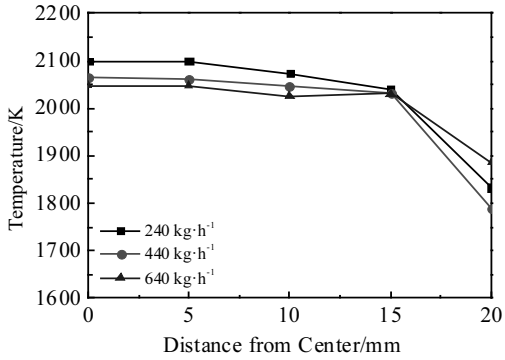

Fig.12 Effect of melting rate on the melt temperature

taken into account. The heat flux on the surface of melt is considered homogeneous. So, melt temperature is determined only by melting power and melting rate. As the result of surface tension gradient of the melt caused by temperature gradient, melt has the tendency to flow to the side wall. At the same time, melt flows from the inlet to the outlet. The real flow of the melt is the superposition of the two movements. Flow field and melt temperature were calculated as shown in Fig.10 to Fig.12.

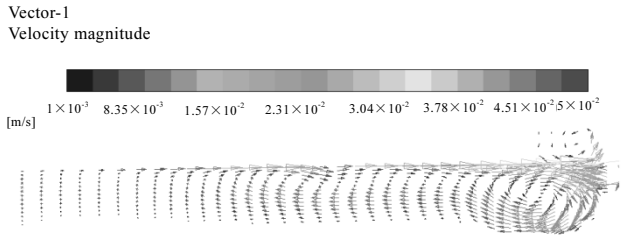

Fig.10 Numerical 3D representation of flow field (intersection A-A′)

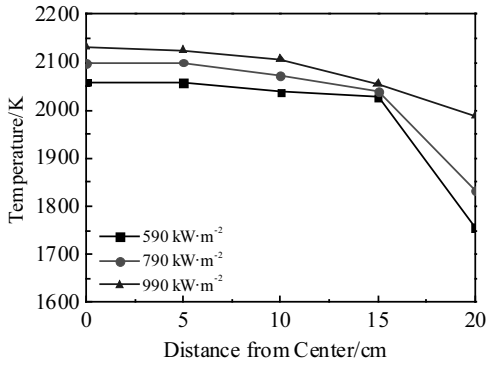

Fig.11 Effect of melting power on the melt temperature

Fig.10 shows that the melt velocity is about a few centimeters per second. The flow of the melt essentially has such characteristics, namely the melt on the surface of the molten pool moves from the center to the edge of the cold hearth. After contacting with the wall, it moves in the opposite direction into internal melt and is accompanied by an ascending motion. The interchange of melt on the surface and in the internal is strong. This is because fluid in the melt has two velocity components, namely, the component pointing to the side wall and the component along the longitudinal direction. This kind of flow is very good for the removal of inclusions, which will be discussed specifically.

Fig.11 and Fig.12 indicate that the melt temperature increases with the increase of melting power and decreases with the increase of melting rate. This is because the melt temperature at the tip of the raw material is lower than that in the hearth. When melting rate increases, more energy is consumed for heating the melt with low temperature.

2.2 Inclusions trajectories

Inclusions in titanium alloys can be classified into two categories. Low density inclusions (LDI) are caused by contamination of nitrogen, oxygen, and carbon. This kind of inclusions mainly comes from titanium sponge, the adding wastes and alloy and improper melting operation. Wherein TiN is most harmful because its density is close to that of the matrix metal. It has the same crystal structure with titanium, so it is difficult to detect. High density inclusions (HDI) are mainly caused by elements with high melting point such as tungsten, molybdenum, tantalum and niobium and mainly come from cutting tools.

As referred previously, EBCHM furnace has excellent capabilities of removing inclusions. If melting parameters are appropriate, inclusions can be totally removed by the cold hearth. In the present work, the migrating behavior of inclusions with different densities and sizes in the hearth was calculated, as shown in Fig.13 and Fig.14.

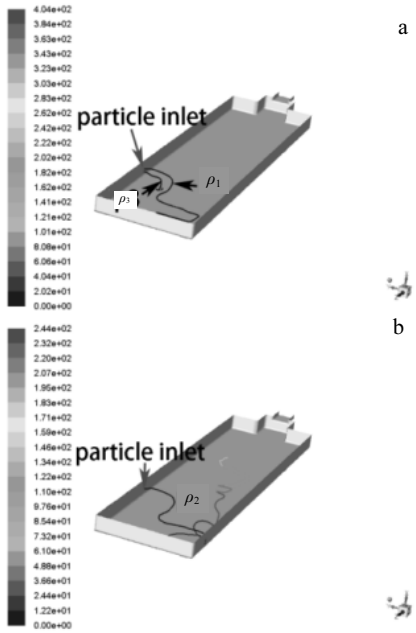

Fig.13 Trajectories of particles of 300 μm in diameter colored with residence time: (a) low density and high density; (b) medium density (ρ_1-4000 kg·m^{-3}, ρ_2-4440 kg·m^{-3}, ρ_3-5000 kg·m^{-3})

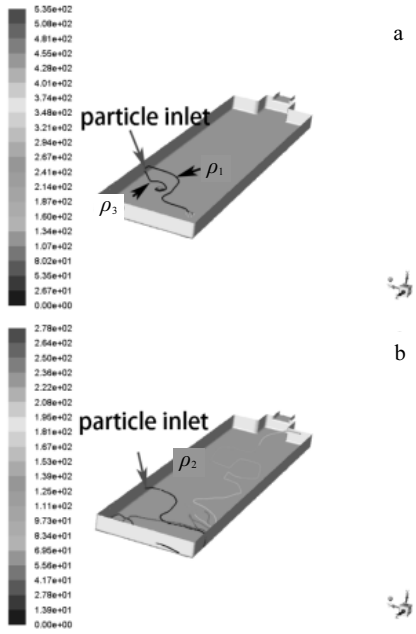

Fig.14 Trajectories of particles of 600 μm in diameter colored with residence time: (a) low density and high density; (b) medium density (ρ_1-4000 kg·m^{-3}, ρ_2-4440 kg·m^{-3}, ρ_3-5000 kg·m^{-3})

It can be seen from Fig.13 and Fig.14 that the migrating trajectories of particles with different sizes have similar behavior. Namely, low density inclusions (ρ_1) are mainly on the surface layer and close to the side wall. Medium density inclusions (ρ_2) flow in a wide range and have very complex trajectories. High density inclusions (ρ_3) drop to the bottom of melt pool directly when it enters into the melt. As the effect of surface tension, inclusions have a component velocity pointing to side wall. So low density inclusions will migrate to the side wall and are removed. Medium density inclusions cannot be totally removed by the effect of pining of shell. The dissolving is the main mechanism of removing for medium density inclusions. As the dissolving process is very slow, it is the main difficulty of removing inclusions. High density inclusions can be removed by the interaction with the bottom of shell.

2.3 Ingot composition

The effect of melting parameters on ingot compositions was calculated by the evaporation model established previously and the cold hearth furnace shown in Fig.5. The results are shown in Fig.15~Fig.17.

Fig.15 shows that the aluminum content decreases and the vanadium content increases with the increase of melting temperature.

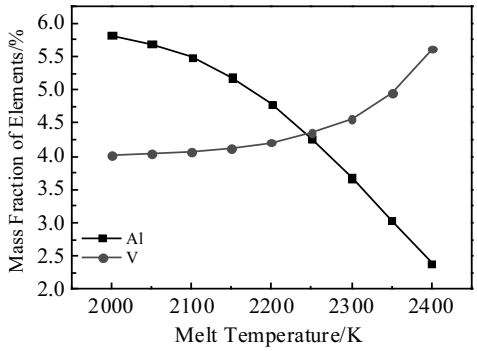

Fig.15 Influence of temperature on the ingot composition (raw material is Ti-6Al-4V, melting rate is 405 kg·h^{-1})

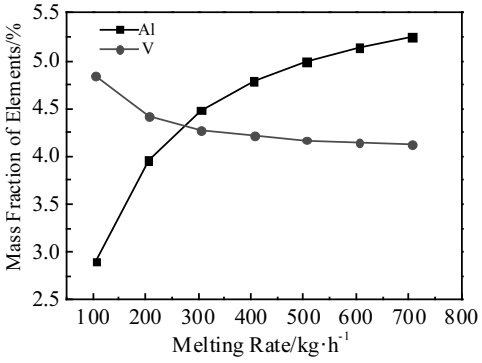

Fig.16 Influence of melting rate on the ingot composition (raw material is Ti-6Al-4V, melting temperature is 2200 K)

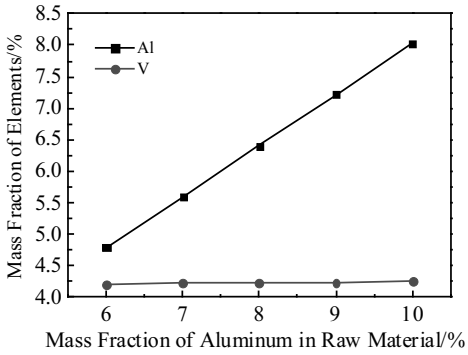

Fig.17 Influence of mass fraction of aluminum in raw material on the ingot composition (melting temperature is 2200 K, melting rate is 405 kg·h^{-1})

Fig.16 indicates that the aluminum content increases and the vanadium content decreases with the increase of melting rate.

Fig.17 shows that aluminum content increases linearly with the increase of aluminum content of the raw material. However, the vanadium content almost does not change.

The experimental investigation of melting Ti-6Al-4V alloy using EBCHM was conducted to validate the theoretical predictions. The EBCHM furnace is shown in Fig.5. The main parameters are shown in Table 2.

A round ingot with the size of Φ260 mm×8100 mm (the 1# ingot) was produced, as shown in Fig.18. The ingot was sliced at the center and a disk with a thickness of 10mm was get. Point 1 was used for EDS analysis and the results show that the composition in the radical direction is relatively homogeneous. Point 2 was used to chemical analysis, and the testing results are shown in Table 3. It can be seen that the calculated value accords well with the experimental value.

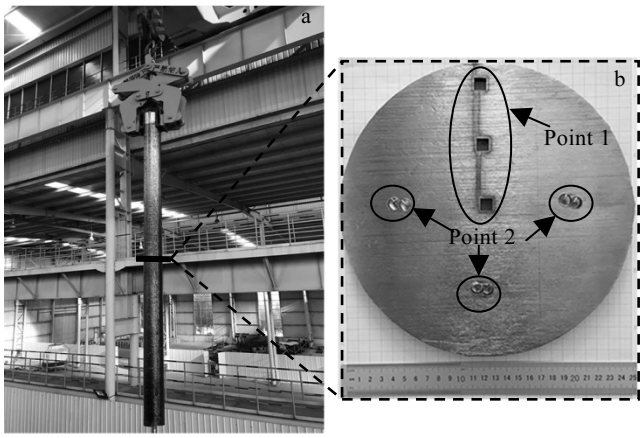

Fig.18 1# ingot (a) and sampling points (b)

According to the previous researches, composition of raw materials is a parameter which is easy to adjust. Based on the evaporation model, the composition of raw material was adjusted to Ti-7.9Al-4V. A round ingot with the size of Φ260 mm×1966 mm (the 2# ingot) was produced using the same melting parameters of the 1# ingot. Using the similar sampling method and testing method of the 1# ingot, the 2# ingot compositions are shown in Table 4.

Table 4 indicates that the ingot composition is very close to the normal composition of Ti-6Al-4V, which means that controlling ingot composition by adjusting the raw materials composition is appropriate.

Table 3 Composition of 1# ingot calculated and detected

Raw material	Ti-9Al-4V
Calculated value	Ti-6.83Al-4.42V
Tested value	Ti-6.90Al-4.76V

Table 4 Composition of 2# ingot calculated and detected

Raw material	Ti-7.9Al-4V
Calculated value	Ti-6.06Al-4.34V
Experimental value	Ti-6.05Al-4.16V

3 Conclusions

1) The melt in the hearth is constrained to a very shallow depth which is about 15 mm in our experiment. The melt velocity in the cold hearth is a few centimeters per second. The melt depth increases with the increase of melting power while the influence of melting rate on the morphology of melt pool is not obvious.

2) The melt temperature increases with the increase of melting power while decreases with the increase of melting rate.

3) Low density inclusions mainly move on the surface layer of melt and are close to the side wall. Medium density inclusions have very complex trajectories and move in a wide range. High density inclusions drop to the bottom of melt pool directly which enters into the melt.

4) The evaporation model used to predict ingot composition for commercial EBCHM furnace is effective. Controlling ingot composition by adjusting the raw materials composition is reasonable.

References

1 William D B, Bird R K, Terryl A W. *Materials Science and Engineering A*[J], 1998, 243: 299

2 Immarigeon J P, Holt R T, Koul A K *et al*. *Materials Characterization*[J], 1995, 35: 41

3 Shima E H, Liu Yujing *et al*. *Materials and Design*[J], 2016, 97: 279

4 Guo Jingjie, Liu Yuan. *Metallurgical and Materials Transactions B*[J], 2000, 31: 837
5 Suzuki K. *Metals and Materials International*[J], 2001, 7: 587
6 Mitchell A. *Materials Science and Engineering A*[J], 1999, 263: 217
7 Zhang Yingming, Zhou Lian, Sun Jun *et al*. *Rare Metal Materials and Engineering*[J], 2008, 37(11): 1973 (in Chinese)
8 Zhang Yingming, Sun Jun, Han Mingchen *et al*. *Aerospace Materials & Technology*[J], 2007:50 (in Chinese)
9 Paton B E, Trigub N P, Zhuk G V. *Materials Science*[J], 2008, 44(3): 328
10 Watakabe S, Suzuki K, Nishikawa K. *ISIJ International*[J], 1992, 32(5): 625
11 Shuster R, Reilly C, Maijer D M *et al. IOP Conference Series: Materials Materials Science and Engineering*[J], 2012, 33: 1
12 Isawa T, Nakamura H, Murakami K. *ISIJ International*[J], 1992, 32(5): 607
13 Bellot J P, Hess E, Ablitzer D. *Metallurgical and Materials Transactions B*[J], 2000, 31(4): 845
14 Lee P D, Quested P N, Mclean M. *Philosophical Transactions*[J], 1998: 1027
15 Bellot J P, Defay B, Jourdan J *et al*. *Journal of Materials Engineering and Performance*[J], 2012, 21: 2140
16 Bellot J P, Foster B, Hans S *et al. Metallurgical and Materials Transactions B*[J], 1996, 28: 1997
17 Han Mingchen, Zhang Yingming, Zhou Yigang *et al*. *Rare Metal Materials and Engineering*[J], 2008, 37(4): 665 (in Chinese)
18 Ghassan G, Pierre C, Alian J *et al*. *ISIJ International*[J], 2012, 52 (1): 1
19 Akhonin S V, Trigub N P, Zamkov V N *et al. Metallurgical and Materials Transactions B*[J], 2003, 34(4): 447
20 Liang Yingjiao, Che Mengchang, Liu Xiaoxia *et al. Thermochemical Properties of Inorganic Substance*[M]. Shenyang: Northeastern University Press, 1993: 1 (in Chinese)
21 Schneider S, Egry I, Seyhan I. *International Journal of Thermophysics*[J], 2002, 23(5): 1241
22 Kobryn P A, Semiatin S L. *Metallurgical and Materials Transactions B*[J], 2001, 32(4): 685
23 Jiang Guangrui, Liu Yuan, Li Yanxiang. *Acta Metallurgica Sinica*[J], 2007, 43(5): 503 (in Chinese)

电子束冷床炉熔炼 Ti-6Al-4V 合金过程中流动、传热和挥发计算

岑孟江, 刘 源, 陈 祥, 张华伟, 李言祥
（清华大学 先进成形制造技术教育部重点实验室, 北京 100084）

摘 要：研究了Ti-6Al-4V合金在电子束冷床炉熔炼(EBCHM)过程中冷床部分熔体的传热、流动和凝固过程。结果表明，冷床部分的熔体被限制在一个非常浅的深度，实验测量约为15 mm，熔体速度大约是每秒几厘米。熔体温度随着熔炼功率增加而升高，随着熔炼速率增加而降低。熔池深度随着熔炼功率升高而增加，而熔炼速率对熔池形貌的影响不明显。模拟了不同密度、不同尺寸夹杂物的运动轨迹。结果表明，夹杂密度对轨迹影响较大。同时建立了元素挥发的数学模型，并研究了熔炼工艺参数对铸锭成分的影响。结果表明，熔炼温度、熔炼速率和原料配比对铸锭成分均有较大影响。采用工业用电子束冷床炉生产了圆锭，测量了冷床凝壳的形貌并检测了铸锭成分。计算结果与实验结果吻合较好。

关键词：EBCHM：Ti-6Al-4V；模拟；挥发

作者简介：岑孟江, 男，1993年生，硕士, 清华大学材料学院, 北京 100084，E-mail:1274217858@qq.com